Progress In Electromagnetics Research, PIER 37, 289–317, 2002

SCATTERING OF A PLANE WAVE BY 1-DIMENSIONAL DIELECTRIC ROUGH SURFACES STUDY OF THE FIELD IN A NONORTHOGONAL COORDINATE SYSTEM

R. Dusséaux and C. Baudier

Université de Versailles Saint-Quentin en Yvelines
Centre d'étude des Environnements Terrestre et Planétaires (CETP)
UMR 8639, 10-12 Avenue de l'Europe, 78140 Vélizy, France

Abstract—We present a rigorous method giving the field scattered by a dielectric plane surface with a local cylindrical perturbation illuminated by a plane wave. The theory is based on Maxwell's equations written in a nonorthogonal coordinate system. A Method of Moments (PPMoM) with Pulses for basis and weighting functions is applied for solving in the spectral domain. For several deterministic profiles, we study the influence of polarization, incidence angle and perturbation depth and show that the distance defining the far-field approximation depends on the observation angle.

1 Introduction

2 Presentation of the Problem

3 Fourier-Rayleigh Integral
- 3.1 Asymptotic Expression
- 3.2 Power Conservation — Scattering Pattern

4 Analysis in the Spectral Domain
- 4.1 Components of Fields and Eigenvalue Systems
- 4.2 Elementary Wave Functions
- 4.3 Scattering Amplitudes and Boundary Conditions
- 4.4 Normalized Power Density

5 Results
- 5.1 Convergence of the Method
- 5.2 Study of Finite Gratings Having a Small Number of Grooves

5.3 Influence of the Deformation Depth
5.4 Distance Associated with the Radiation Zone

6 Conclusion

Appendix A. Power Balance for a Lossless Dielectric Interface

References

1. INTRODUCTION

We present a method giving the field scattered by a dielectric plane surface with a cylindrical local perturbation illuminated by a plane wave in $E_{\parallel}$ or $H_{\parallel}$ polarization. The method is based on Maxwell's equations in covariant form written in the translation nonorthogonal coordinate system [1–3]. The principle of resolution has been presented in [4] for the case of perfectly conducting surfaces. In this paper, we adapt the method to dielectric media (Sections 2–4). In the translation coordinate system and for each medium, the covariant components of the electric vector and magnetic vector fulfill an eigenvalue system. A Method of Moments (PPMoM) with Pulses for basis and weighting functions is applied for solving these systems in the spectral domain [5]. The Fourier transforms of fields are expanded in series of pulse functions $\hat{b}_q(\alpha)$. The width $\Delta\alpha$ of the basis functions defines the spectral resolution. Using an inner product, eigenvalue systems are projected over functions $\hat{b}_q(\alpha)$. Finally, for each medium, a scattering matrix is obtained, the size of which is fixed by the truncation order M. The eigenvalues of these matrices and the corresponding eigenvectors lead to elementary wave functions. For each medium, the scattered field is expanded as a linear combination of eigensolutions satisfying the outgoing wave condition. Their amplitudes are found by solving the boundary conditions. Outside the modulated zone, the longitudinal covariant components of the reflected field and transmitted field can be represented by a superposition of a continuous spectrum of outgoing plane waves, the so-called Fourier-Rayleigh integral [6–9]. For a lossless dielectric material, the far-field and the scattering pattern can be derived from the asymptotic approximation of the Fourier-Rayleigh integrals [8].

In Section 5, for several deterministic profiles, we study the influence of polarization, incidence angle and of perturbation depth and show that the distance which determines the radiation zone depends on the observation angle. We also show some comparisons with a

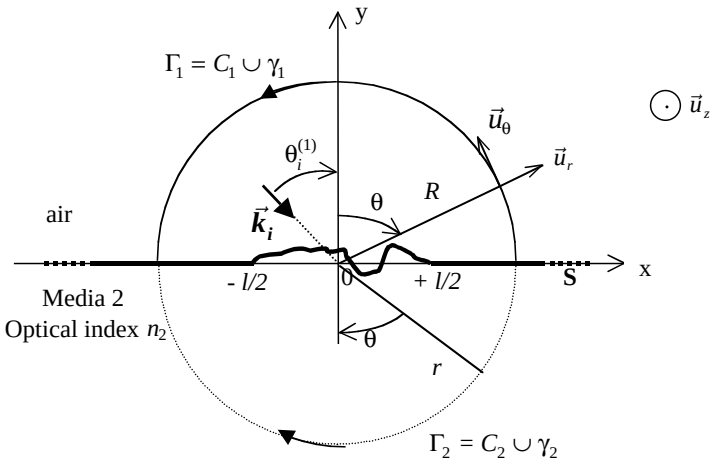

Figure 1. Plane with a local deformation illuminated by a plane wave under incidence $\theta_i^{(1)}$. According to the conventions used here, $\theta_i^{(1)}$ and θ are positive.

Rayleigh method in order to confirm its numerical applicability domain presented in [8, 9].

2. PRESENTATION OF THE PROBLEM

In Fig. 1, we consider a local perturbation in a dielectric plane surface. The deformation is given by the equation $y = a(x)$, where $a(x)$ is a local function defined over the interval $[-l/2; l/2]$, where l is the width of the modulated zone. The surface separates the air (medium 1, $n_1 = 1$) from a dielectric material with a real or complex refractive index n_2 (medium 2). This structure is illuminated under incidence $\theta_i^{(1)}$ by a monochromatic plane wave of wavelength λ. The incident wave vector $\vec{k}_i$ lies in the xOy plane. Both fundamental cases of polarization $E_\parallel$ and $H_\parallel$ are considered. For $E_\parallel$ polarization, the electric vector is parallel to the Oz axis and for $H_\parallel$ polarization, this is the case for the magnetic vector (Eq. 1). The time-dependence factor is in $\exp(j\omega t)$, where ω is the angular frequency. Afterwards, any vector function is represented by its associated complex vector function and the time factor is suppressed. Upper or lower indices (1) and (2) denote

quantities relative to medium 1 and medium 2, respectively.

$$F_{0-}^{(1)}(x,y) = \exp(-j\alpha_i x + j\beta_i^{(1)} y) = \begin{cases} E_{z,0-}^{(1)}(x,y) & \text{in} E_{\|} \\ Z_1 H_{z,0-}^{(1)}(x,y) & \text{in} H_{\|} \end{cases} \tag{1a}$$

$$\alpha_i = k_i \sin\theta_i^{(1)};\ \ \beta_i^{(1)} = k_1 \cos\theta_i^{(1)};\ \ k_1 = |\vec{k}_1| = \frac{2\pi}{\lambda};\ \ Z_1 = \sqrt{\frac{\mu_0}{\varepsilon_0}} \approx 120\pi \tag{1b}$$

In the absence of a deformation, the total field $F_0^{(1)}(x,y)$ in medium 1 is the sum of the incident field $F_{0-}^{(1)}(x,y)$ and the specularly reflected field $F_{0+}^{(1)}(x,y)$:

$$F_0^{(1)} = F_{0-}^{(1)}(x,y) + F_{0+}^{(1)}(x,y) \tag{2a}$$

$$F_{0+}^{(1)}(x,y) = \rho^{(1)} \exp(-j\alpha_i x - j\beta_i^{(1)} y) = \begin{cases} E_{z,0+}^{(1)}(x,y) & \text{in } E_{\|} \\ Z_1 H_{z,0+}^{(1)}(x,y) & \text{in } H_{\|} \end{cases} \tag{2b}$$

and the total field $F_0^{(2)}(x,y)$ in medium 2 is reduced to the transmitted field $F_{0-}^{(2)}(x,y)$:

$$\begin{aligned} F_0^{(2)}(x,y) = F_{0-}^{(2)}(x,y) &= \rho^{(2)} \exp(-j\alpha_i x + j\beta_i^{(2)} y) \\ &= \begin{cases} E_{z,0-}^{(2)}(x,y) & \text{in } E_{\|} \\ Z_2 H_{z,0-}^{(2)}(x,y) & \text{in } H_{\|} \end{cases} \end{aligned} \tag{2c}$$

with

$$\beta_i^{(2)} = \sqrt{k_2^2 - \alpha_i^2};\quad k_2 = n_2 k_1;\quad Z_2 = Z_1/n_2 \tag{2d}$$

If

$$\mathrm{Im}(n_2) = 0,\quad \beta_i^{(2)} = k_2 \cos\theta_i^{(2)} \tag{2e}$$

$F_{0-}^{(1,2)}(x,y)$ designates a plane wave moving in direction $-y$ and $F_{0+}^{(1,2)}(x,y)$, one moving in direction $+y$, respectively. $\rho^{(1)}$ and $\rho^{(2)}$ are the Fresnel reflection and transmission coefficients, respectively,

defined as follows:

$$\rho_{E_\parallel}^{(1)} = \frac{\beta_i^{(1)} - \beta_i^{(2)}}{\beta_i^{(1)} + \beta_i^{(2)}} \qquad \text{and} \qquad \rho_{E_\parallel}^{(2)} = \frac{2\beta_i^{(1)}}{\beta_i^{(1)} + \beta_i^{(2)}} \tag{3a}$$

$$\rho_{H_\parallel}^{(1)} = \frac{\dfrac{\beta_i^{(1)}}{n_1^2} - \dfrac{\beta_i^{(2)}}{n_2^2}}{\dfrac{\beta_i^{(1)}}{n_1^2} + \dfrac{\beta_i^{(2)}}{n_2^2}} \qquad \text{and} \qquad \rho_{H_\parallel}^{(2)} = \frac{n_1}{n_2} \frac{2\dfrac{\beta_i^{(1)}}{n_1^2}}{\dfrac{\beta_i^{(1)}}{n_1^2} + \dfrac{\beta_i^{(2)}}{n_2^2}} \tag{3b}$$

If $\mathrm{Im}(n_2) = 0$ and $n_1 = 1$, $\rho^{(1)}$ and $\rho^{(2)}$ are real.

For a locally deformed plane, we consider, in addition to the incident, reflected and transmitted plane waves, a scattered field $F_d^{(1,2)}(x,y)$. The plane waves $F_{0\mp}^{(1,2)}(x,y)$ have an infinite power but the scattered fields $F_d^{(1,2)}(x,y)$ have a finite power and a zero mean power density per unit surface [8, 9]. The problem consists in working out the field $F_d^{(1,2)}(x,y)$ scattered within the two media.

3. FOURIER-RAYLEIGH INTEGRAL

3.1. Asymptotic Expression

Outside the deformation, the scattered field can be represented by a superposition of a continuous spectrum of outgoing plane waves [6–9], the so-called Fourier-Rayleigh integral (4).

For $y > y_M^{(1)} = \max(a(x))$ and $y < y_M^{(2)} = \min(a(x)),\ \forall x$,

$$\begin{aligned} F_d^{(m)}(x,y) &= \frac{1}{2\pi} \int_{-\infty}^{+\infty} \hat{R}^{(m)}(\alpha) \exp(-j\beta^{(m)}(\alpha)|y|) \exp(-j\alpha x) d\alpha \\ &= \begin{cases} E_{d,z}^{(m)}(x,y) \text{ in } E_\parallel \\ \text{or} \\ Z_m H_{d,z}^{(m)}(x,y) \text{ in } H_\parallel \end{cases} \end{aligned} \tag{4}$$

In a lossless medium (m), a propagating wave is defined when $|\alpha| < k_m$, with:

$$\alpha = k_m \sin\theta; \quad \beta^{(m)}(\alpha) = \sqrt{k_m^2 - \alpha^2} = k_m \cos\theta \ \text{ and } \ -\pi/2 < \theta < \pi/2 \tag{5a}$$

An evanescent wave exists when $|\alpha| \geq k_m$ with:

$$\beta^{(m)}(\alpha) = -j\sqrt{k_m^2 - \alpha^2} \tag{5b}$$

In the far-field zone, the Fourier-Rayleigh integral is reduced to the only contribution of the propagating waves. In the polar coordinate system, we show that the asymptotic expression of the Fourier-Rayleigh integral is given by [8]:

$$\begin{aligned}\vec{F}_d^{(m)}&(x = r\sin\theta, y = r\cos\theta)\\ &\approx \left(\frac{1}{2\pi}\int_{-k_m}^{+k_m} \hat{R}^{(m)}(\alpha)\exp(-j\beta^{(m)}(\alpha)|y|)\exp(-j\alpha x)d\alpha\right)\vec{u}_z\\ &= \left(F_{d_{\text{far}}}^{(m)}(r,\theta) + O\left(\frac{1}{r^{3/2}}\right)\right)\vec{u}_z \end{aligned} \tag{6a}$$

$$F_{d_{\text{far}}}^{(m)}(r,\theta) = \sqrt{\frac{k_m}{2\pi r}}\hat{R}^{(m)}(k_m\sin\theta)\cos\theta\exp(-jk_m r)\exp\left(j\frac{\pi}{4}\right) \tag{6b}$$

In the radiation zone, the field $F_{d_{\text{far}}}^{(m)}(r,\theta)$ at the observation point (r,θ) decreases as $1/\sqrt{r}$ and the angular dependence is given by the function $\hat{R}^{(m)}(\alpha)\cos\theta$, and becomes identified with the propagating wave amplitudes of the continuous spectrum (4) with $\alpha = k_m\sin\theta$.

3.2. Power Conservation — Scattering Pattern

For a lossless material, the angular power density $\frac{dP_d^{(m)}(\theta)}{d\theta}$ is defined as follows:

$$\frac{dP_d^{(m)}(\theta)}{d\theta} = \frac{k_m|\hat{R}^{(m)}(k_m\sin\theta)|^2\cos^2(\theta)}{4\pi Z_m} \quad \text{with} \quad -\pi/2 < \theta < +\pi/2 \tag{7}$$

$dP_d^{(m)}(\theta)$ is the real part of the flux of the complex scattered Poynting vector of the scattered field $F_{d_{\text{far}}}^{(m)}(r,\theta)$ through an elementary surface $d\vec{S} = rd\theta\Delta z\vec{u}_r$, with $\Delta z = 1$. The angular power density $\frac{dP_d^{(m)}(\theta)}{d\theta}$ (W.rad^{-1}) defines the scattering pattern.

Many authors [12] define an angular density of scattered power in degrees normalized with respect to the flux of incident power through

the modulated region:

$$\frac{d\xi_d^{(m)}(\theta)}{d\theta} = \frac{\pi}{180 P_i} \frac{dP_d^{(m)}(k_m \sin\theta)}{d\theta} = \frac{\pi}{180\lambda l} \frac{n_m^2 |\hat{R}^{(m)}(k_m \sin\theta)|^2 \cos^2\theta}{\cos\theta_i^{(1)}} \tag{8}$$

where $-90° < \theta < +90°$ with

$$P_i = \frac{1}{2} \operatorname{Re}\left(\int_{-l/2}^{+l/2} \vec{E}_{0-}^{(1)} \wedge \vec{H}_{0-}^{(1)^*} dx \right), \quad \vec{u}_y = \frac{1}{2Z_1} l \cos\theta_i^{(1)} \tag{9}$$

h^* is the complex conjugate of h and $\vec{a} \wedge \vec{b}$ the vector product of $\vec{a}$ and $\vec{b}$. $\frac{d\xi_d^{(1)}(-\theta_i^{(1)})}{d\theta}$ is the backscattering coefficient of the surface illuminated under incidence $\theta_i^{(1)}$.

For lossless dielectric media, $\hat{R}^{(m)}(k_m \sin\theta)$ fulfils the power balance criterion (10) where $\xi_d^{(m)}$ corresponds to the total normalized power scattered in medium (m) and $\xi_0^{(m)}$ represents the electromagnetic coupling between the reference field $F_0^{(m)}$ and the scattered field $F_d^{(m)}$ (Appendix A).

$$\xi_d^{(1)} + \xi_d^{(2)} = \xi_0^{(1)} + \xi_0^{(2)} \tag{10a}$$

and

$$\xi_0^{(m)} = -\frac{2}{l} \frac{n_m \cos\theta_i^{(m)}}{\cos\theta_i^{(1)}} \rho^{(m)} \operatorname{Re}\left[\hat{R}^{(m)}(k_m \sin\theta_i^{(m)})\right] \tag{10b}$$

The accuracy on the power balance can be defined as follows:

$$\Delta\xi = -\log_{10}\left(\frac{\xi_d^{(1)} + \xi_d^{(2)} - \xi_0^{(1)} - \xi_0^{(2)}}{\xi_d^{(1)} + \xi_d^{(2)}} \right) \tag{11}$$

The integer part of $\Delta\xi$ gives the number of significant digits common to $\xi_d^{(1)} + \xi_d^{(2)}$ and $\xi_0^{(1)} + \xi_0^{(2)}$. The relative error on the power balance (10) is equal to $10^{-\Delta\xi}$.

4. ANALYSIS IN THE SPECTRAL DOMAIN

The scattered field cannot be expressed by the Rayleigh integral in the modulated zone ($Y_M^{(2)} < y < Y_M^{(1)}$) if the perturbation amplitude is

too large [6–9]. In this paper, we propose to derive an expression of electromagnetic fields that is valid everywhere in space, outside and on the surface, by solving Maxwell's equations in the translation coordinate system $(x, u = y - a(x), z)$ [1–3].

4.1. Components of Fields and Eigenvalue Systems

If there is no current density and no charge density, then under their covariant form [1, 3], Maxwell's equations expressed in the translation system lead to a differential system:

$$\frac{1}{jk_m}\frac{\partial F^{(m)}(x,u)}{\partial u} = \frac{d(x)}{jk_m}\frac{\partial F^{(m)}(x,u)}{\partial x} + \big(c(x)-1\big)G^{(m)}(x,u) \quad (12a)$$

$$\frac{1}{jk_m}\frac{\partial G^{(m)}(x,u)}{\partial u} = \frac{1}{k_m^2}\frac{\partial}{\partial x}\left[c(x)\frac{\partial F^{(m)}(x,u)}{\partial x}\right] - \frac{1}{k_m^2}\frac{\partial^2 F^{(m)}(x,u)}{\partial x^2} - F^{(m)}(x,u) + \frac{1}{jk_m}\frac{\partial}{\partial x}\big[d(x)G^{(m)}(x,u)\big] \quad (12b)$$

The local functions $c(x)$ and $d(x)$ depend on the profile derivative:

$$d(x) = \frac{\dot{a}(x)}{1+\dot{a}(x)^2}; \quad c(x) = \dot{a}(x)d(x); \quad \dot{a}(x) = \frac{da(x)}{dx} \quad (13)$$

System (12) is valid for the two types of polarization, with for $E_{\parallel}$ polarization:

$$F^{(m)}(x,u) = E_z^{(m)}(x,u); \quad G^{(m)}(x,u) = Z_m H_x^{(m)}(x,u)$$
$$E_x^{(m)}(x,u) = E_u^{(m)}(x,u) = H_z^{(m)}(x,u) = 0 \quad \text{and} \quad H_u^{(m)}(x,u) \neq 0 \quad (14a)$$

for $H_{\parallel}$ polarization:

$$F^{(m)}(x,u) = Z_m H_z^{(m)}(x,u); \quad G^{(m)}(x,u) = -E_x^{(m)}(x,u)$$
$$H_x^{(m)}(x,u) = H_u^{(m)}(x,u) = E_z^{(m)}(x,u) = 0 \quad \text{and} \quad E_u^{(m)}(x,u) \neq 0 \quad (14b)$$

The covariant components $E_x^{(m)}(x,u)$, $E_z^{(m)}(x,u)$, $H_x^{(m)}(x,u)$ and $H_z^{(m)}(x,u)$ are parallel to surfaces u = constant. These components verify the boundary conditions in $u = 0$, hence their presence in differential system (12).

4.2. Elementary Wave Functions

After a positive Fourier transform, system (12) takes the form:

$$\frac{1}{jk_m}\frac{\partial \hat{F}^{(m)}(\alpha,u)}{\partial u} = -\frac{1}{2\pi k_m}\int_{-\infty}^{+\infty}\gamma \hat{d}(\alpha-\gamma)\hat{F}^{(m)}(\gamma,u)d\gamma + \frac{1}{2\pi}\int_{-\infty}^{+\infty}\hat{c}(\alpha-\gamma)\hat{G}^{(m)}(\gamma,u)d\gamma - \hat{G}^{(m)}(\alpha,u) \tag{15a}$$

$$\frac{1}{jk_m}\frac{\partial \hat{G}^{(m)}(\alpha,u)}{\partial u} = -\frac{\alpha}{2\pi k_m^2}\int_{-\infty}^{+\infty}\gamma \hat{c}(\alpha-\gamma)\hat{F}^{(m)}(\gamma,u)d\gamma - \frac{k_m^2-\alpha^2}{k_m^2}\hat{F}^{(m)}(\alpha,u) - \frac{\alpha}{2\pi k_m}\int_{-\infty}^{+\infty}\hat{d}(\alpha-\gamma)\hat{G}^{(m)}(\gamma,u)d\gamma \tag{15b}$$

$\hat{F}^{(m)}(\alpha,u)$, $\hat{G}^{(m)}(\alpha,u)$, $\hat{c}(\alpha)$ and $\hat{d}(\alpha)$ are the Fourier transforms of functions $F^{(m)}(x,u)$, $G^{(m)}(x,u)$, $c(x)$ and $d(x)$, respectively.

A method of moments with pulses as basis and weighting functions is applied to solve system (15) in the spectral domain [5]. The unknown functions $\hat{F}^{(m)}(\alpha,u)$ and $\hat{G}^{(m)}(\alpha,u)$ and the Fourier transforms $\hat{c}(\alpha)$ and $\hat{d}(\alpha)$ are expanded in a series of piecewise functions (pulses) $\hat{b}_q(\alpha)$ of unit amplitude, of width $\Delta\alpha$, and centered on $\alpha_q = q\Delta\alpha$:

$$\hat{F}^{(m)}(\alpha,u) = \sum_{q=-\infty}^{q=+\infty} F_q^{(m)}(u)\hat{b}_q(\alpha); \quad \hat{G}^{(m)}(\alpha,u) = \sum_{q=-\infty}^{q=+\infty} G_q^{(m)}(u)\hat{b}_q(\alpha) \tag{16}$$

$$\hat{c}(\alpha) = \sum_{q=-\infty}^{q=+\infty} c_q\hat{b}_q(\alpha); \qquad \hat{d}(\alpha) = \sum_{q=-\infty}^{q=+\infty} d_q\hat{b}_q(\alpha) \tag{17}$$

The spectral resolution $\Delta\alpha$ is fixed by the cut-off integer M_c.

$$\Delta\alpha = \frac{2k_1}{2M_c+1} \tag{18}$$

The basis functions constitute an orthonormal basis with respect to the inner product (19) where $\delta_{m,q}$ denotes the Kronecker symbol.

$$\left\langle \hat{b}_m(\alpha); \hat{b}_q(\alpha)\right\rangle = \int_{-\infty}^{+\infty}\hat{b}_m(\alpha)\hat{b}_q(\alpha)d\alpha = \Delta\alpha\delta_{m,q} \tag{19}$$

Substituting expressions (16) and (17) into system (15) and taking the inner product of the intermediate equations with each basis function $\hat{b}_q(\alpha)$, we obtain, for each medium, an infinite system of differential equations relating coefficients $F_q^{(m)}(u)$ and $G_q^{(m)}(u)$ to each other. With a truncation order M, the resolution gives $4M+2$ eigensolutions of initial system (15):

$$\hat{F}_n^{(m)}(\alpha,u) = \sum_{q=-M}^{q=+M} f_{qn}^{(m)} \hat{b}_q(\alpha) \exp(jk_m r_n^{(m)}|u|)$$
$$\text{with} \quad 1 \leq n \leq 4M+2 \tag{20}$$
$$\hat{G}_n^{(m)}(\alpha,u) = \sum_{q=-M}^{q=+M} g_{qn}^{(m)} \hat{b}_q(\alpha) \exp(jk_m r_n^{(m)}|u|)$$

where $f_{qn}^{(m)}$ and $g_{qn}^{(m)}$ with $-M \leq q \leq M$ represent the components of eigenvectors $\vec{f}_n^{(m)}$ and $\vec{g}_n^{(m)}$ associated with the eigenvalue $r_n^{(m)}$.

The principle of resolution has been briefly described in this subsection. This principle is detailed in [4] for a perfectly conducting interface. Nevertheless, the expressions of matrices given in [4] are valid whatever the refractive index of medium.

The signs of the real (Re) and imaginary (Im) parts of $k_m r_n^{(m)}$ define the nature of the wave corresponding to the elementary wave function (20). In particular, $\hat{F}_n^{(m)}(\alpha,u)$ and $\hat{G}_n^{(m)}(\alpha,u)$ represent an outgoing wave propagating without attenuation if $\mathrm{Re}(k_m r_n^{(m)}) < 0$ and $\mathrm{Im}(k_m r_n^{(m)}) = 0$. For an evanescent wave, $\mathrm{Im}(k_m r_n^{(m)}) > 0$.

In [4], we show that the eigenvalues are opposite two by two. Since r_n and $-r_n$ are eigenvalues, among the $4M+2$ eigenfunctions (20), there are $2M+1$ of them that correspond to outgoing waves and as many of them to incoming waves.

For lossless media, the real eigenvalues are on the interval $[-1;+1]$ and correspond to the cosine of scattering angles. Moreover, among the $2M+1$ outgoing waves, $2\,\mathrm{Ent}(n_m M_c + n_m/2)+1$ are moving without attenuation and give the far-field (Ent designates the integer part).

Finally, the Fourier transforms of covariant components of scattered fields are defined as a linear combination of $2M+1$ eigensolutions

(20) satisfying the outgoing wave condition.

$$\hat{F}_d^{(m)}(\alpha,u) = \sum_{n=1}^{2M+1} A_n^{(m)} \hat{F}_n^{(m)}(\alpha,u) \tag{21a}$$

$$\hat{G}_d^{(m)}(\alpha,u) = \sum_{n=1}^{2M+1} A_n^{(m)} \hat{G}_n^{(m)}(\alpha,u) \tag{21b}$$

4.3. Scattering Amplitudes and Boundary Conditions

The scattering amplitudes A_n are found by solving the boundary conditions in $u=0$ (i.e., in $y=a(x)$). Taking into account expressions (1) and (2) of the longitudinal component $F_0^{(m)}(x,y)$ of the total field without any deformation and expressions (21) of covariant components of the scattered field, we obtain:
For $E_\parallel$ polarization:

$$F_d^{(1)}(x,u=0) - F_d^{(2)}(x,u=0) = -F_0^{(1)}\big(x,y=a(x)\big) + F_0^{(2)}\big(x,y=a(x)\big) \tag{22a}$$

$$\begin{aligned}\frac{G_d^{(1)}(x,u=0)}{Z_1} - \frac{G_d^{(2)}(x,u=0)}{Z_2} &= -\left(-\frac{1}{jk_1Z_1}\frac{\partial F_0^{(1)}(x,y)}{\partial y} + \dot{a}(x)\frac{1}{jk_1Z_1}\frac{\partial F_0^{(1)}(x,y)}{\partial x}\right)_{y=a(x)} \\ &\quad + \left(-\frac{1}{jk_2Z_2}\frac{\partial F_0^{(2)}(x,y)}{\partial y} + \dot{a}(x)\frac{1}{jk_2Z_2}\frac{\partial F_0^{(2)}(x,y)}{\partial x}\right)_{y=a(x)}\end{aligned} \tag{22b}$$

For $H_\parallel$ polarization:

$$\frac{F_d^{(1)}(x,u=0)}{Z_1} - \frac{F_d^{(2)}(x,u=0)}{Z_2} = -\frac{F_0^{(1)}\big(x,y=a(x)\big)}{Z_1} + \frac{F_0^{(2)}\big(x,y=a(x)\big)}{Z_2} \tag{23a}$$

$$\begin{aligned}-G_d^{(1)}(x,u=0) + G_d^{(2)}(x,u=0) &= -\left(\frac{1}{jk_1}\frac{F_0^{(1)}(x,y)}{\partial y} - \dot{a}(x)\frac{1}{jk_1}\frac{\partial F_0^{(1)}(x,y)}{\partial x}\right)_{y=a(x)} \\ &\quad + \left(\frac{1}{jk_2}\frac{\partial F_0^{(2)}(x,y)}{\partial y} - \dot{a}(x)\frac{1}{jk_2}\frac{\partial F_0^{(2)}(x,y)}{\partial x}\right)_{y=a(x)}\end{aligned} \tag{23b}$$

After a Fourier transform, the continuity relations (22) and (23) are projected onto the basis functions. According to (1), (2), (20) and (21), for each polarization, a $(4M+2)$-dimensional matrix system is obtained, the inversion of which leads to spectral amplitudes $A_n^{(m)}$. For $E_\parallel$ polarization and $-M \leq q \leq +M$:

$$\sum_{n=1}^{2M+1} A_n^{(1)} f_{qn}^{(1)} - \sum_{n=1}^{2M+1} A_n^{(2)} f_{qn}^{(2)} = -\left(S_{0-,q}^{(1)} + \rho_{E_\parallel}^{(1)} S_{0+,q}^{(1)}\right) + \rho_{E_\parallel}^{(2)} S_{0+,q}^{(2)} \quad (24a)$$

$$\begin{aligned} &\frac{1}{Z_1}\sum_{n=1}^{2M+1} A_n^{(1)} g_{qn}^{(1)} - \frac{1}{Z_2}\sum_{n=1}^{2M+1} A_n^{(2)} g_{qn}^{(2)} \\ &\quad = \frac{k_1}{\beta_i^{(1)} Z_1}\left(S_{0-,q}^{(1)} - \rho_{E_\parallel}^{(1)} S_{0+,q}^{(1)}\right) - \frac{\alpha_i}{\beta_i^{(1)} k_1 Z_1}\left(T_{0-,q}^{(1)} - \rho_{E_\parallel}^{(1)} T_{0+,q}^{(1)}\right) \\ &\quad\quad - \frac{k_2 \rho_{E_\parallel}^{(2)}}{\beta_i^{(2)} Z_2} S_{0-,q}^{(2)} + \frac{\alpha_i \rho_{E_\parallel}^{(2)}}{\beta_i^{(2)} k_2 Z_2} T_{0-,q}^{(2)} \end{aligned} \quad (24b)$$

For $H_\parallel$ polarization and $-M \leq q \leq +M$:

$$\frac{1}{Z_1}\sum_{n=1}^{2M+1} A_n^{(1)} f_{qn}^{(1)} - \frac{1}{Z_2}\sum_{n=1}^{2M+1} A_n^{(2)} f_{qn}^{(2)} = -\frac{1}{Z_1}\left(S_{0-,q}^{(1)} + \rho_{H_\parallel}^{(1)} S_{0+,q}^{(1)}\right) + \frac{\rho_{H_\parallel}^{(2)}}{Z_2} S_{0q}^{(2)} \quad (25a)$$

$$\begin{aligned} &\sum_{n=1}^{2M+1} A_n^{(1)} g_{qn}^{(1)} - \sum_{n=1}^{2M+1} A_n^{(2)} g_{qn}^{(2)} \\ &\quad = \frac{Z_1 k_1}{\beta_i^{(1)}}\left(S_{0-,q}^{(1)} - \rho_{H_\parallel}^{(1)} S_{0+,q}^{(1)}\right) - \frac{Z_1 \alpha_i}{\beta_i^{(1)} k_1}\left(T_{0-,q}^{(1)} - \rho_{H_\parallel}^{(1)} T_{0+,q}^{(1)}\right) \\ &\quad\quad - \frac{Z_2 k_2 \rho_{H_\parallel}^{(2)}}{\beta_i^{(2)}} S_{0-,q}^{(2)} + \frac{Z_2 \alpha_i \rho_{H_\parallel}^{(2)}}{\beta_i^{(2)} k_2} T_{0-,q}^{(2)} \end{aligned} \quad (25b)$$

The coefficients of second members of Eqs. (24) and (25) are given by:

$$S_{0\mp,q}^{(m)} = \frac{1}{\Delta\alpha}\int_{-l/2}^{l/2}\left(\exp\left(\pm j\beta_i^{(m)} a(x)\right) - 1\right) I_q^*(x)\exp(-j\alpha_i x)dx \quad (26a)$$

$$T_{0\mp,q}^{(m)} = \frac{1}{\Delta\alpha}\int_{-l/2}^{l/2}\left(\exp\left(\pm j\beta_i^{(m)} a(x)\right) - 1\right) J_q^*(x)\exp(-j\alpha_i x)dx \quad (26b)$$

Functions $I_q(x)$ and $J_q(x)$ are defined as follows:

$$I_q(x) = \int_{\alpha_q-\Delta\alpha/2}^{\alpha_q+\Delta\alpha/2} \exp(-j\alpha x)d\alpha = \Delta\alpha \,\mathrm{sinc}\left(\Delta\alpha\frac{x}{2}\right)\exp(-j\alpha_q x) \quad (27a)$$

$$\begin{aligned} J_q(x) &= \int_{\alpha_q-\Delta\alpha/2}^{\alpha_q+\Delta\alpha/2} \alpha\exp(-j\alpha x)d\alpha \\ &= \frac{\exp(-j\alpha_q x)}{jx}\left(2j\alpha_q \sin\left(\Delta\alpha\frac{x}{2}\right) + \Delta\alpha\,\mathrm{sinc}\left(\Delta\alpha\frac{x}{2}\right)\right. \\ &\quad \left. - \Delta\alpha\cos\left(\Delta\alpha\frac{x}{2}\right)\right) \end{aligned} \quad (27b)$$

4.4. Normalized Power Density

$\frac{d\xi_d^{(m)}}{d\theta}$ is defined from the scattering amplitudes $\hat{R}^{(m)}(\alpha)$ (Eqs. 4 and 8). Outside the modulated zone, the longitudinal components $F_d^{(m)}(x,u)$ can be represented by the Fourier-Rayleigh integrals. For a lossless medium, the following continuity relations can then be written:
At $y = y_M^{(m)},\ \forall x$

$$\begin{aligned} &F_d^{(m)}\left(x, u = y_M^{(m)} - a(x)\right) \\ &\quad = \frac{1}{2\pi}\int_{-\infty}^{+\infty} \hat{R}^{(m)}(\alpha)\exp\left(-j\beta^{(m)}(\alpha)\left|y_M^{(m)}\right|\right)\exp(-j\alpha x)d\alpha \end{aligned} \quad (28)$$

The function $\hat{R}^{(m)}(\alpha)$ is obtained by solving the continuity relation (28) with the PPMo method in the spectral domain [4]. Projections $R_q^{(m)}$ of $\hat{R}^{(m)}(\alpha)$ onto the basis functions $\hat{b}_q(\alpha)$ are given by:
$\forall q \in [-M; +M]$,

$$R_q^{(m)} = \frac{\exp\left(+j\beta_q^{(m)}\left|y_M^{(m)}\right|\right)}{\Delta\alpha}\sum_{n=1}^{2M+1}\left(V_{qn}^{(m)} + f_{qn}^{(m)}\right)\exp\left(jk_m r_n^{(m)}\left|y_M^{(m)}\right|\right)A_n^{(m)} \quad (29)$$

with

$$V_{qn}^{(m)} = \sum_{p=-M}^{+M} f_{pn}^{(m)}\int_{-l/2}^{l/2}\left(\exp\left(j(-1)^m k_m r_n^{(m)} a(x)\right) - 1\right) I_p^*(x) I_q(x)dx \quad (30)$$

$$\beta_q^{(m)} = \left(\langle \hat{b}_q(\alpha);\ (k_m^2 - \alpha^2)\hat{b}_q(\alpha)\rangle\right)^{1/2}$$
$$= k_1 \left(n_m^2 - \frac{12q^2+1}{3(2M_c+1)^2}\right)^{1/2};\quad \mathrm{Im}(\beta_q^{(m)}) \le 0 \qquad (31)$$

5. RESULTS

5.1. Convergence of the Method

M_c and M are the two numerical parameters of the method. The cut-off integer M_c sets the width $\Delta\alpha$ of pulses $\hat{b}_q(\alpha)$. As M_c increases, $\Delta\alpha$ decreases and the approximation of functions $\hat{F}_d(\alpha, u)$, $\hat{G}_d(\alpha, u)$, $\hat{c}(\alpha)$ and $\hat{d}(\alpha)$ in series (16) and (17) becomes more accurate. The consequence of the M^{th}-order truncation is the suppression of high spatial frequency evanescent waves in the Fourier transform of field components (21) and in Rayleigh integrals (4). Indeed, integration variable α varies within interval $[-\alpha_{\max}; +\alpha_{\max}]$ where $\alpha_{\max}$ depends on ratio M/M_c:

$$\alpha_{\max} = \alpha_M = M\Delta\alpha = \frac{2k_1 M}{2M_c+1} \approx k_1 \frac{M}{M_c} \quad \text{if} \quad M_c \gg 1 \qquad (32)$$

The method is numerically stable and the accuracy in the results increases with M and M_c. The convergence tests proposed in [4] for the case of perfectly conducting surfaces can be applied to dielectric interfaces and the two main conclusions remain valid:

- For a given wavelength λ and a given depth, the value M_c increases with the length of the deformation (the value of the spectral resolution $\Delta\alpha$ ensuring the numerical convergence decreases with l).
- For given λ and l values, the value of $\alpha_{\max}$ ensuring the convergence of results increases with the depth of the deformation.

5.2. Study of Finite Gratings Having a Small Number of Grooves

The finite grating under consideration [10, 11] is a rough surface whose profile is given by:

$$a(x) = -h\cos\left(\frac{2\pi x}{D}\right) V(x) \qquad (33a)$$

with:

$$V(x) = \begin{cases} 0 & \text{if } |x| > +\dfrac{l}{2} \\ 1 & \text{if } -\dfrac{l}{2} + t < x < +\dfrac{l}{2} - t \\ \dfrac{x + l/2}{t} - \dfrac{1}{2\pi} \sin\left(\dfrac{2\pi}{t}\left(x + \dfrac{l}{2}\right)\right) & \text{if } -\dfrac{l}{2} < x < -\dfrac{l}{2} + t \\ \dfrac{l/2 - x}{t} - \dfrac{1}{2\pi} \sin\left(\dfrac{2\pi}{t}\left(\dfrac{l}{2} - x\right)\right) & \text{if } \dfrac{l}{2} - t < x < \dfrac{l}{2} \end{cases} \tag{33b}$$

Figure 2 shows four finite gratings with $t = D/2$ and $h = 0.2D$. The length l is equal to 3, 5, 7 and $9D$, respectively. Figure 3 and Figure 4 give the normalized power density $\frac{d\xi_d^{(m)}}{d\theta}$ associated with these 4 lengths ($\theta_i^{(1)} = 30°$, $\lambda = 0.9D$, $n_2 = 3/2$).

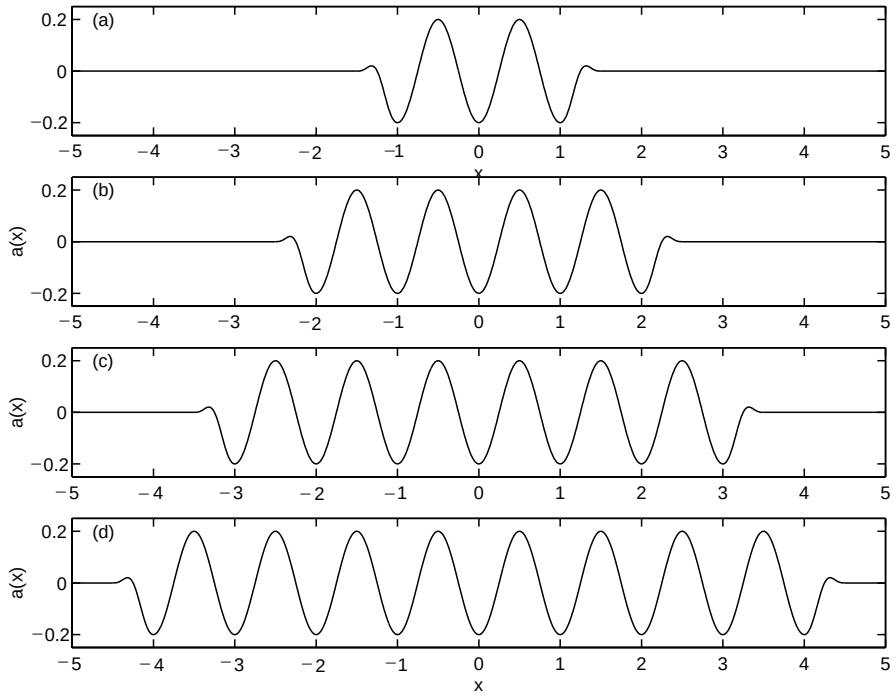

Figure 2. Finite gratings having a small number of grooves. $t = D/2$ and $h = 0.2D$. From top to the bottom, $l = 3,\ 5,\ 7,\ 9D$ with $D = 1\,\text{m}$.

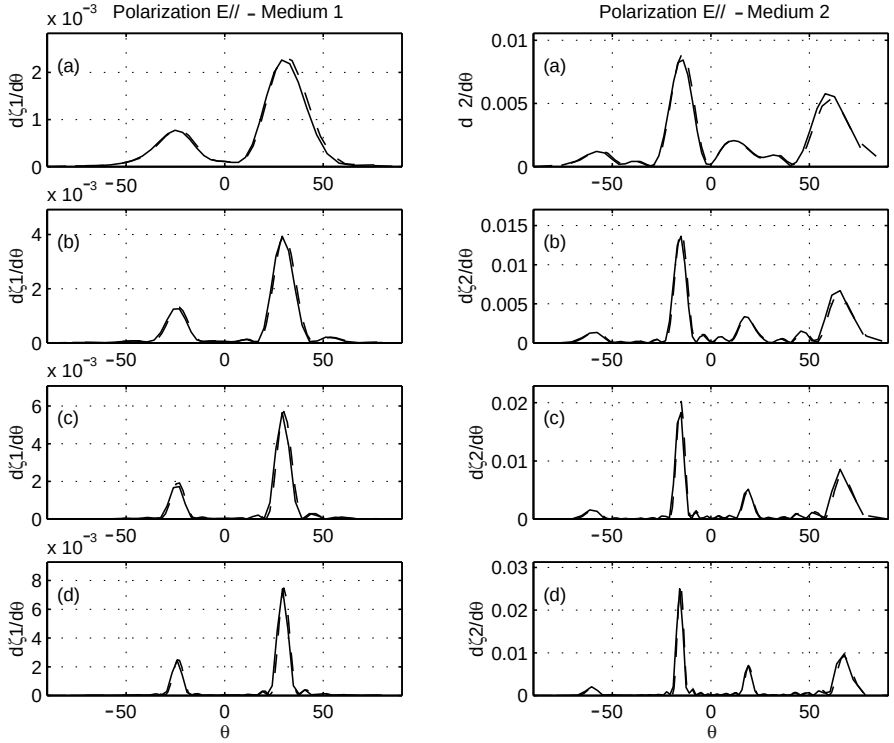

Figure 3. Normalized scattering pattern for $E_{\|}$ polarized finite grating referenced in Subsection 5.2. $\theta_i^{(1)} = 30°$, $\lambda = 0.9D$, $n_2 = 3/2$, $\theta_i^{(1)} = 0°$ and $P_i = \frac{l-2t}{2Z_1}\cos\theta_i^{(1)}$. For profile (a), $(M_c; M) = (16; 80)$. For profiles (b) and (c), $(M_c; M) = (20; 100)$. For profile (d), $(M_c; M) = (24; 120)$. The dashed curves show the values given by the Rayleigh method [8, 9].

The obvious conclusion is that the ratio of lobe amplitudes is nearly independent of the number of grooves since $l \geq 5D$. These peaks correspond to the scattering angles of the infinite grating. Moreover, the width of lobes is in inverse ratio to the number of grooves. For all these structures, the normalized powers $\xi_d^{(1)}$ and $\xi_d^{(2)}$ scattered in the two media are of the order of 0.07 and 0.57 for the $E_{\|}$ case and 0.05 and 0.35 for the $H_{\|}$ case, respectively. Insofar as $\xi_d^{(1)}$ and $\xi_d^{(2)}$ values are constant and as the width of peak varies as $1/l$, we deduce that the height of these peaks is proportional to the number of grooves, a

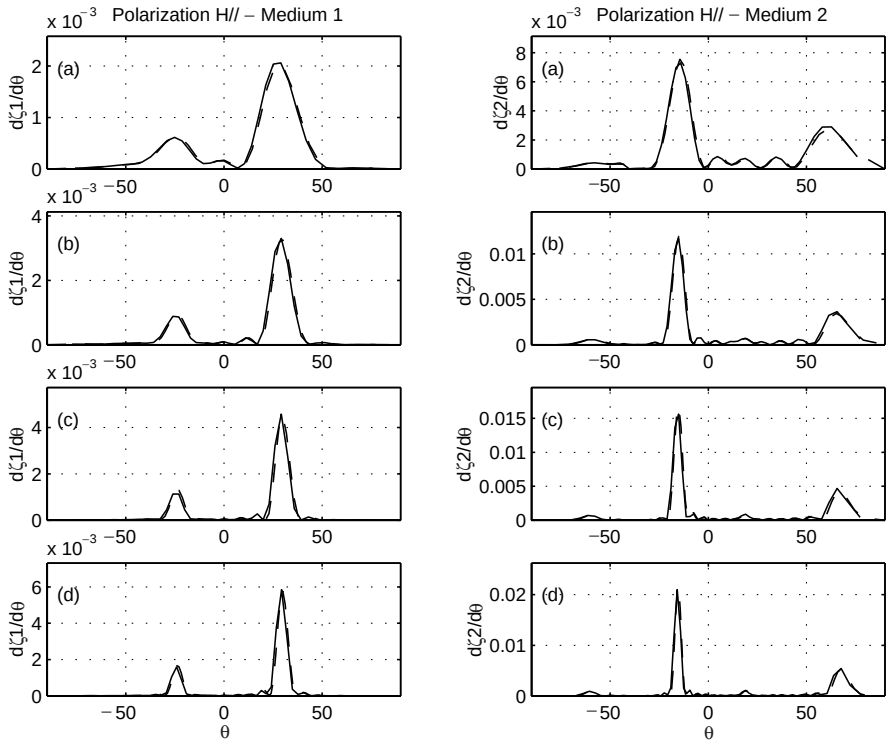

Figure 4. Normalized scattering pattern for $H_{\|}$ polarized finite grating referred to in Subsection 5.2. Same values as in Fig. 3.

fact which can be confirmed in Figures 3 and 4.

The value of M_c depends on the lobe width of the scattering pattern. M_c sets the spectral resolution $\Delta\alpha$ and consequently, the angular resolution. One should increase the cut-off integer value for a better description of narrow lobes. For the profiles under consideration, M_c increases with l. For example, for $l = 3D$ and $l = 9D$, we take $M_c = 16$ and $M_c = 24$, respectively. With $h = 0.2D$ and $\lambda = 0.9D$, the depth of gratings is 0.44λ. Taking $M = 5M_c$, formula (31) gives $\alpha_{\max} \approx 5k_1 = 10k_2/3$. This value ensures a good description of the scattered field inside and outside the grooves. With these values of M_c and M, the errors on the power balance (11) are smaller than 10^{-3}.

Figures 3 and 4 also show the scattering patterns obtained by a Rayleigh method [8, 9]. We have recently determined the numerical applicability domain of this method in the far=field zone [8, 9] and we try to confirm this domain. Here, the surfaces under consideration are

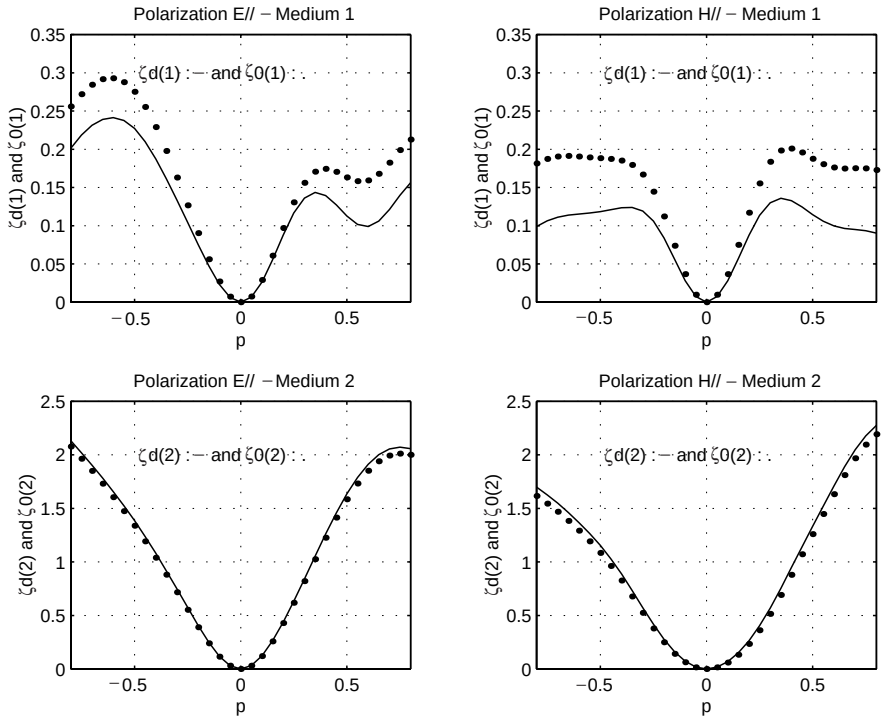

Figure 5. Total normalized power scattered in medium (m) $\xi_d^{(m)}$ and normalized coupling power $\xi_0^{(m)}$ as a function of the depth parameter p for the profile referred to in Subsection 5.3. $M_c = 16$, $M = \mathrm{Ent}(|p|/\lambda + 2)M_c$; $l = D = 20\,\mathrm{cm}$, $\lambda = 10\,\mathrm{cm}$, $\theta_i^{(1)} = 17.6°$, $n_2 = 1.94$.

included in or very close to the domain and the comparisons with the rigorous method are quite good. The reliability of the results obtained by the Rayleigh method is confirmed. Nevertheless, the power balance errors increase with l. For $l = 3D$, this error is smaller than 10^{-2}. For $l = 9D$, it is close to 1.5% in $E_{\|}$, and 4% in $H_{\|}$.

5.3. Influence of the Deformation Depth

Figure 5 shows the normalized scattered powers $\xi_d^{(m)}$ and the normalized coupling powers $\xi_0^{(m)}$ as a function of the parameter p defining the

deformation depth:

$$a(x) = \begin{cases} \dfrac{p\lambda}{2}\left(\cos\left(\dfrac{2\pi x}{D}\right) + \cos\left(\dfrac{4\pi x}{D}\right)\right) & \text{if } |x| \leq \dfrac{l}{2} \\ 0 & \text{if } |x| > \dfrac{l}{2} \end{cases} \tag{34}$$

with $l = D = 20\,\text{cm}$, $\lambda = 10\,\text{cm}$, $\theta_i = 17.6°$, $n_2 = 1.94$ and $-0.8 \leq p \leq +0.8$.

For $p = \pm 0.8$, the perturbation has a depth equal to $5\lambda/4$. With $p = 0$, the surface is reduced to a plane and the scattered fields are zero. The obvious conclusion is that the normalized scattered powers $\xi_d^{(m)}$ do not increase systematically with the depth. For $E_\parallel$ polarization, the maximum of $\xi_d^{(1)}$ is reached at $p = -0.55$ and for $H_\parallel$ polarization at $p = +0.4$.

For these profiles, $M_c = 16$ is used and the truncation order increases with depth. For $p = 4/10$, $M = 6M_c$ and for $p = 8/10$, $M = 10M_c$, i.e., $\alpha_{\max} \approx 6k_1$ and $\alpha_{\max} \approx 10k_1$, respectively. In all cases, the power balance is obtained with an error smaller than 10^{-3}.

Figure 6 gives the scattering patterns in air, associated with 4 $(-p; +p)$ pairs for $E_\parallel$ polarization. Figure 7 shows the scattering patterns associated with same values of p but in the dielectric material and for $H_\parallel$ polarization. Patterns given for $p = -0.2$ and $p = +0.2$ are almost superimposed. With these values, the $y = a(x)$ and $y = -a(x)$ profiles represent small-depth perturbations which can be analyzed with the Small Perturbation method [12, 13]. With the SP approximation, for a given deformation, $\frac{d\xi_d^{(m)}(\theta)}{d\theta}$ is proportional to the square modulus of the profile Fourier transform in $\alpha = k_m \sin\theta - k_1 \sin\theta_i^{(1)}$. Consequently, for a small depth versus the wavelength, the scattering patterns for the $y = a(x)$ and $y = -a(x)$ profiles are equal.

From the comparison with the rigorous method, we note that the Rayleigh method gives reliable results in both polarizations and for both media below $|p| = 0.6$, but, it fails drastically for $p = \pm 0.8$. These observations are in accordance with the numerical applicability domain: with $l = 2\lambda$, the Rayleigh method is fully capable of accurately describing the far field produced by local perturbations having amplitudes close to λ and a derivative with an absolute value smaller than $5/2$.

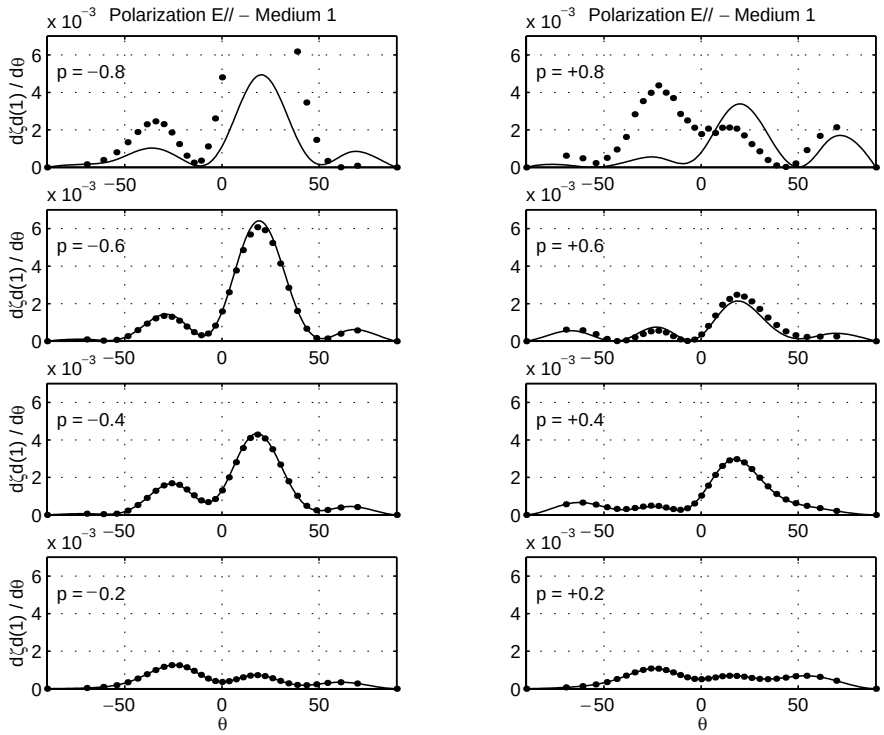

Figure 6. Normalized scattering patterns $\frac{d\xi_d^{(1)}}{d\theta}$ for four values of $\pm p$ of $E_{\parallel}$ polarized profiles referred to in Subsection 5.3. The dashed curves show the values given by the Rayleigh method [8, 9]. Same values as in Fig. 5.

5.4. Distance Associated with the Radiation Zone

The deformation under consideration is described by a Schwartz function:

$$a(x) = \begin{cases} 0 & \text{if } |x| > l/2 \\ h \exp\left(b - \dfrac{bl^2}{l^2 - 4x^2}\right) & \text{if } |x| \leq l/2 \end{cases} \qquad (35)$$

$$\text{with } l = 2\lambda;\ h = 0.4\lambda;\ b = 2$$

Figure 8 gives the Oz component magnitudes of the scattered field and of the far field as a function of the distance from the origin, r, for an observation angle $\theta = 42°$ and under an incidence $\theta_i^{(1)} = 20°$

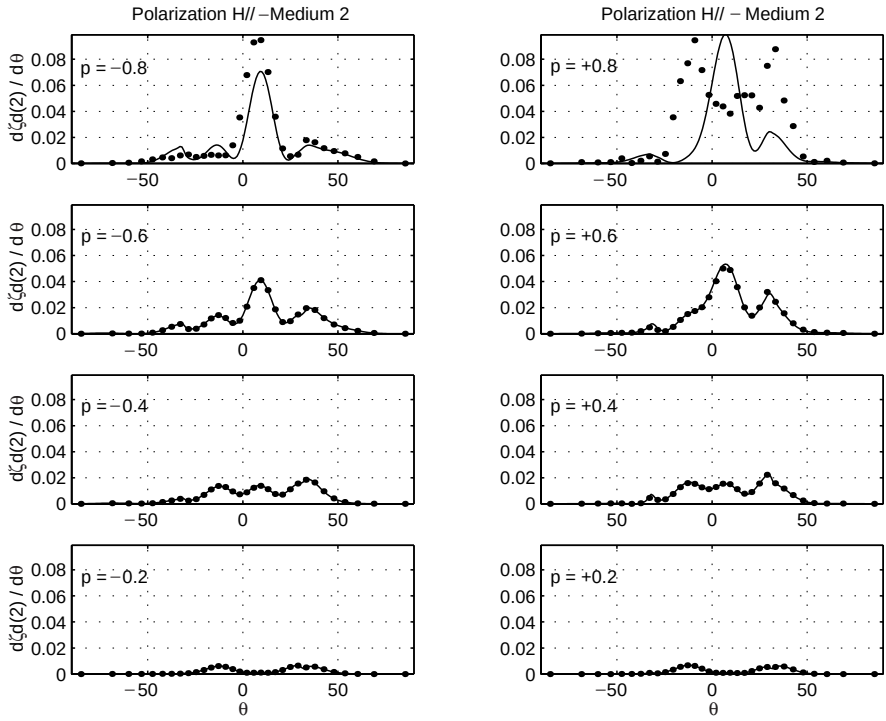

Figure 7. Normalized scattering patterns $\frac{d\xi_d^{(2)}}{d\theta}$ for four values of $\pm p$ of $H_{\|}$ polarized profiles referred to in Subsection 5.3. Same values as in Fig. 5.

($\lambda = 1\,\mathrm{m}$, $n_2 = 1.5$). The asymptotic field $F_{d_{\mathrm{far}}}^{(m)}(r,\theta)$ is given by (6b). The spatial-domain values of the longitudinal component of scattered fields $F_d^{(m)}(x,u)$ is obtained by an inverse Fourier transform of (20a) and (21a):

$$F_d^{(m)}(x,u) = \frac{\sin(\Delta\alpha x/2)}{\pi x} F_{dp}^{(m)}(x,u) \tag{36a}$$

$$F_{dp}^{(m)}(x,u) = \sum_{n=1}^{2M+1} A_n^{(m)} \sum_{q=-M}^{+M} f_{qn}^{(m)} \exp(-jq\Delta\alpha x) \exp(jk_m r_n^{(m)}|u|) \tag{36b}$$

with $u = y - a(x)$.

The expression in cylindrical coordinates is obtained from Eq. (36) with $x = r\sin\theta$ and $y = r\cos\theta$. On all the curves shown, the

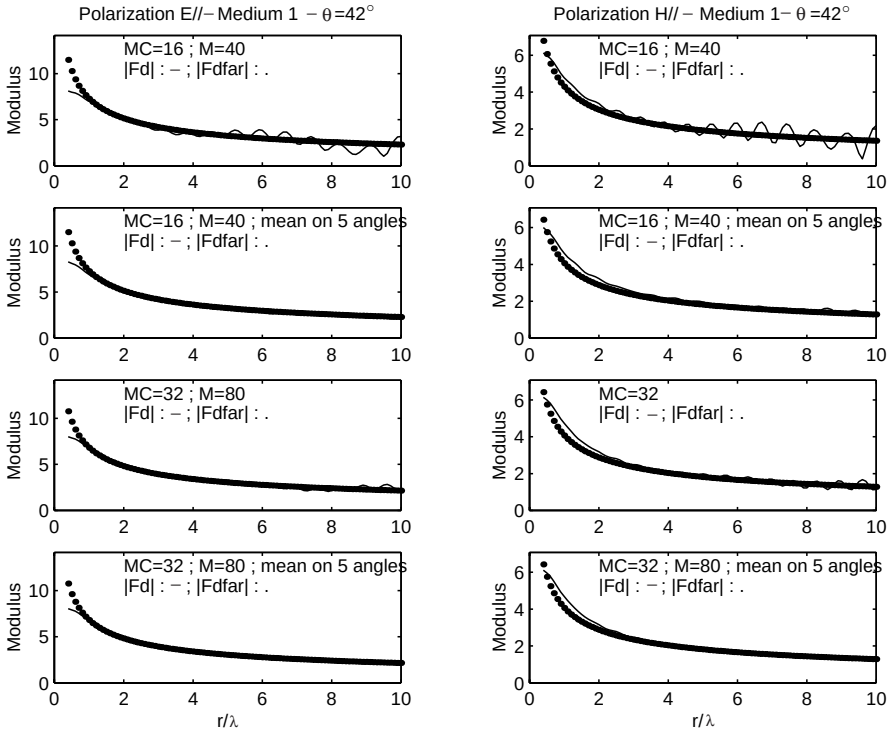

Figure 8. Magnitude and phase of $F_d^{(1)}(r,\theta)$ and $F_{d_{\text{far}}}^{(1)}(r,\theta)$ as a function of r under the observation angle $\theta = 42°$ for the Schwartz profile referred to in Subsection 5.4. $l = 2\lambda$, $h = 0.4\lambda$; $b = 2$, $\theta_i^{(1)} = 20°$; $\lambda = 1\,\text{m}$ and $n_2 = 1.5$.

cosine of observation angles in the lossless medium (m) corresponds to eigenvalues $r_n^{(m)}$. In this case, the asymptotic field amplitude $\hat{R}^{(m)}(\alpha = k\sin\theta)$ corresponds to one of the projection coefficients $R_q^{(m)}$ of $\hat{R}^{(m)}(\alpha)$ onto the basis function $\hat{b}_q(\alpha)$.

Function $F_d^{(m)}(x,u)$ (Eq. 36) is defined as the product of the periodic function $F_{dp}^{(m)}(x,u)$, of period $2\pi/\Delta\alpha$ by the function $\frac{\sin(\Delta\alpha x/2)}{\pi x}$, the main lobe of which has a width of $4\pi/\Delta\alpha$. Then, the curve of the scattered field magnitude can show unwanted oscillations. For a large enough observation distance, sooner or later, these oscillations dominate. Figure 8(a) shows that with $M_c = 16$, these appear from $r = 2.2\lambda$ in $E_{\|}$ polarization, and from $r = 1.4\lambda$ in $H_{\|}$ polarization.

It is important to overcome this drawback. First, we can increase the value of M_c. Figure 8(c) shows that with $M_c = 32$, the phenomenon appears only from $r = 4.4\lambda$ in $E_\parallel$ polarization, and from $r = 2.2\lambda$ in $H_\parallel$ polarization. A reduction of these oscillations can also be obtained by filtering in the angular-domain. Figures 8(b) and 8(d) give the modulus of the mean scattered field over five angles ($Q = 2$ in (37)).

$$\left\langle F_d^{(m)}(r,\theta_n)\right\rangle = \frac{1}{2Q+1}\sum_{q=-Q}^{q=+Q} F_d^{(m)}(r,\theta_{n+q}) \tag{37}$$

θ_n is the observation angle corresponding to an eigenvalue $r_n^{(m)}$, with $r_n^{(m)} = \cos\theta_n$.

This process is effective. For the profile under consideration, with $M_c = 16$, the curves giving the magnitudes of $\langle F_d^{(1)}(r,\theta)\rangle$ and $F_{d_{\text{far}}}^{(1)}(r,\theta)$ are superimposed from an observation distance r that depends on the polarization, until $r = 10\lambda$.

To compare the functions $\langle F_d^{(m)}(r,\theta)\rangle$ and $F_{d_{\text{far}}}^{(m)}(r,\theta)$, a limit distance $d^{(m)}$ is defined as follows:

$$\forall r > d^{(m)}, \quad \left|\frac{\left|\langle F_d^{(m)}\rangle\right| - \left|F_{d_{\text{far}}}^{(m)}\right|}{\left|F_{d_{\text{far}}}^{(m)}\right|}\right| < 0.1 \tag{38}$$

For $r > d^{(m)}$, the relative modulus error between the exact representation $\langle F_d^{(m)}(r,\theta)\rangle$ and the asymptotic approximation $F_{d_{\text{far}}}^{(m)}(r,\theta)$ is smaller than 10%. For an observation angle $\theta = 42°$, $d^{(1)} \approx 0.6\lambda$ in $E_\parallel$ polarization, and $d^{(1)} \approx 1.2\lambda$ in $H_\parallel$ polarization (Fig. 9). Distance $d^{(m)}$ can be seen as the limit between the near zone and the far field zone. For a given observation angle, this limit depends on the incident wave polarization.

Figure 9 gives the magnitude and phase of $\langle F_d^{(2)}(r,\theta)\rangle$ and $F_{d_{\text{far}}}^{(2)}(r,\theta)$ as a function of r in medium (2). For the observation angle $\theta = 0°$, $d^{(2)} \approx 1.4\lambda \approx 0.93\lambda_2$ in $E_\parallel$ polarization, and $d^{(2)} \approx 1.2\lambda \approx 0.8\lambda_2$ in $H_\parallel$ polarization. For $r > d^{(2)}$, the phases of $\langle F_d^{(2)}(r,\theta)\rangle$ (circles) and of $F_{d_{\text{far}}}^{(2)}(r,\theta)$ (dots) are superimposed. Expressions (36–37) are fully capable of accurately describing the near field and the far-field both in magnitude and phase.

Figure 10 gives normalized scattering patterns $\frac{d\xi_d^{(1)}}{d\theta}$ in $E_\parallel$ polarization and $\frac{d\xi_d^{(2)}}{d\theta}$ in $H_\parallel$ polarization and the magnitudes of $\langle F_d^{(m)}(r,\theta)\rangle$

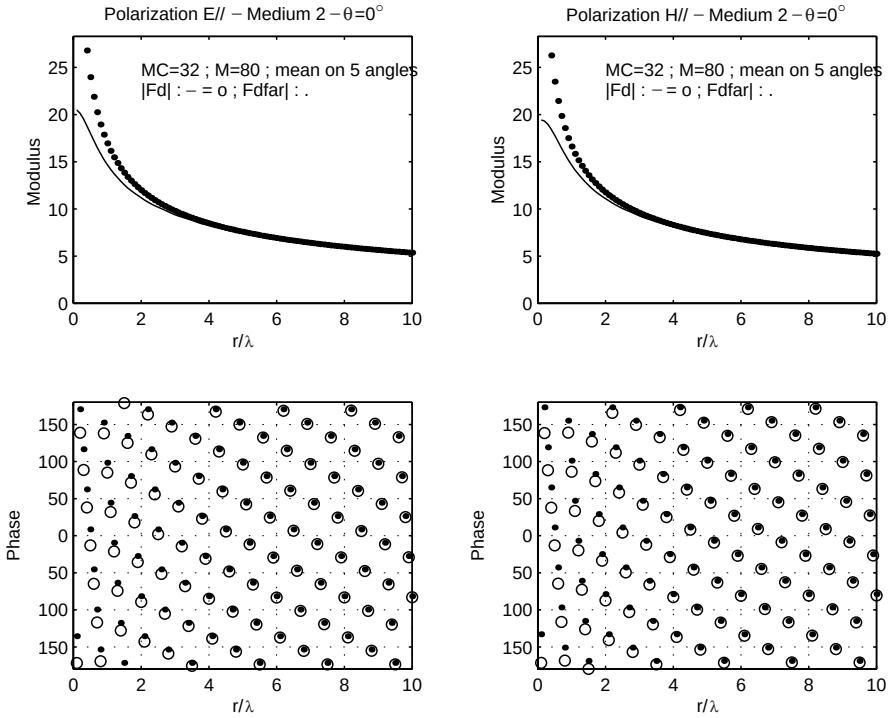

Figure 9. Magnitude and phase of $F_d^{(2)}(r,\theta)$ and $F_{d_{\text{far}}}^{(2)}(r,\theta)$ as a function of r under the observation angle $\theta = 42°$ for the Schwartz profile referred to in Subsection 5.4. Same values as in Fig. 8.

and $F_{d_{\text{far}}}^{(m)}(r,\theta)$ under two observation angles. Table 1 gives the values of $d^{(m)}$ associated with Figures 8, 9 and 10. The obvious conclusion is that for given polarization and medium, $d^{(m)}$ depends on the observation angle. Moreover, $d^{(m)}(\theta)$ does not systematically increase with $\frac{d\xi_d^{(m)}}{d\theta}$. For example, in $E_{\|}$ polarization, the maximum value of $\frac{d\xi_d^{(1)}}{d\theta}$ is obtained in the specular direction $\theta = \theta_i^{(1)} = 20°$ with $\left.\frac{d\xi_d^{(1)}}{d\theta}\right|_{\theta=\theta_i^{(1)}} = 0.0886$ and $d^{(1)}(\theta_i^{(1)}) = 3.2\lambda$. Well then, under $\theta = -27.5°$, $\frac{d\xi_d^{(1)}}{d\theta} = 0.0198$ and $d^{(1)}(\theta) = 3.5\lambda$.

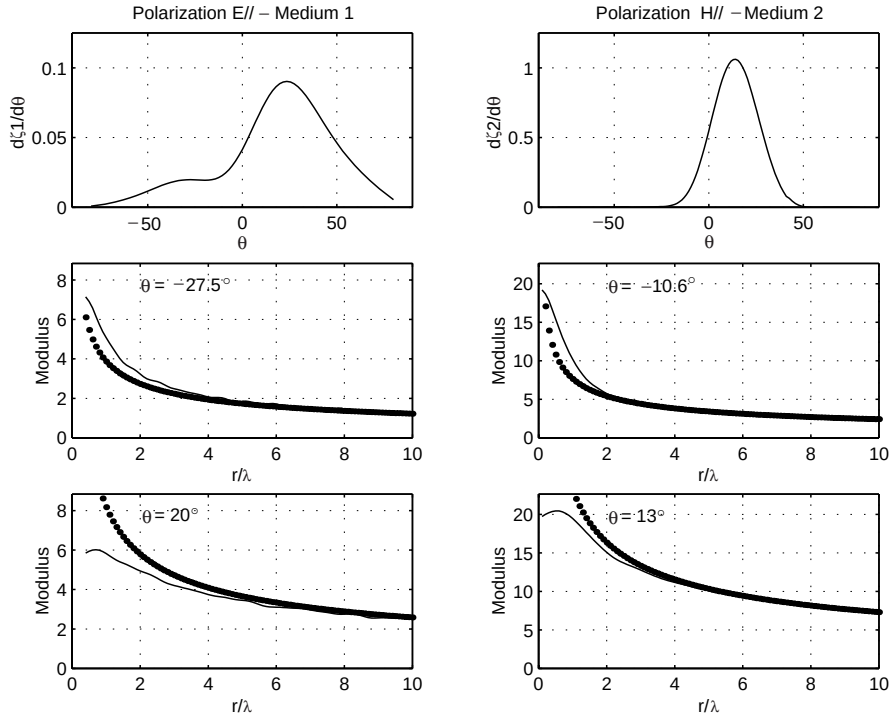

Figure 10. Normalized scattering patterns and magnitudes of $F_d^{(m)}(r,\theta)$ and $F_{d_{\text{far}}}^{(m)}(r,\theta)$ in both media as a function of r under many observation angles. Same values as in Fig. 8.

Table 1. Values of $d^{(m)}$ for different observation angles.

Medium (m)	Polarization	Observation angle	$d^{(m)}/\lambda$
1	$E_{\parallel}$	$-27.5°$	3.5
1	$E_{\parallel}$	$20°$	3.2
1	$E_{\parallel}$	$42°$	0.7
2	$H_{\parallel}$	$-10.6°$	1.9
2	$H_{\parallel}$	$0°$	1.2
2	$H_{\parallel}$	$13°$	1.4

6. CONCLUSION

The method proposed in this paper gives the field scattered by a dielectric plane surface with a local deformation. The method is numerically stable and the accuracy in the results increases with the truncation order M and the cut-off integer M_c [4].

A filtering is applied in the angular-domain to reduce unwanted oscillations inherent to the expression of the scattered field $F_d^{(m)}(r,\theta)$. Accordingly, the method gives the near field and for a lossless dielectric material, it allows the asymptotic behaviour in magnitude and phase to be found.

To compare the filtered field $\langle F_d^{(m)}(r,\theta)\rangle$ and the asymptotic field $F_{d_{\text{far}}}^{(m)}(r,\theta)$, the limit distance $d^{(m)}$ from which the relative modulus error is smaller than 10% is defined. We show that for given polarization and medium, $d^{(m)}$ depends on the observation angle.

APPENDIX A. POWER BALANCE FOR A LOSSLESS DIELECTRIC INTERFACE

We consider the bounded contour $\Gamma_1 = C_1 \cup \gamma$ in Figure 1 where C_1 is a half-circle centered at the origin of radius $R > l/2$ and γ is the part of surface $\mathbf{S}$ for $x \in [-R; R]$. $\Gamma_2 = C_2 \cup \gamma$ is the bounded contour defined in the dielectric material. C_1 is taken in the anticlockwise sense, C_2 in the clockwise sense.

For two lossless dielectric media with $k_2 > k_1$, the second Green identity applied to the longitudinal component of the total field over contour Γ_m yields:

$$\operatorname{Im}\left[\int_{C_m}(F_d^{(m)}+F_0^{(m)})\frac{\partial(F_d^{(m)}+F_0^{(m)})^*}{\partial r}\,Rd\theta + \int_{\gamma}(F_d^{(m)}+F_0^{(m)})\frac{\partial(F_d^{(m)}+F_0^{(m)})^*}{\partial n}\,dl\right]=0 \quad \text{(A1)}$$

$\frac{\partial}{\partial n}$ denotes the differentiation along the outward normal to Γ_m.

In $E_{\parallel}$ polarization, $F_d^{(1)}+F_0^{(1)} = F_d^{(2)}+F_0^{(2)}$ over γ, and taking into account of the directions of C_1 and C_2, according to (A1), we

obtain:

$$\mathrm{Im}\left[\int_{-\pi/2}^{+\pi/2}(F_d^{(1)}+F_0^{(1)})\left(\frac{\partial F_d^{(1)}}{\partial r}+\frac{\partial F_0^{(1)}}{\partial r}\right)^* d\theta + \int_{-\pi/2}^{+\pi/2}(F_d^{(2)}+F_0^{(2)})\left(\frac{\partial F_d^{(2)}}{\partial r}+\frac{\partial F_0^{(2)}}{\partial r}\right)^* d\theta\right]=0 \quad \text{(A2)}$$

Four integrals must be computed. According to (6), a first integral is given by:

$$\mathrm{Im}\left[\int_{-\pi/2}^{+\pi/2}\left(F_d^{(1)}\frac{\partial F_d^{(1)}{}^*}{\partial r}+F_d^{(2)}\frac{\partial F_d^{(2)}{}^*}{\partial r}\right)d\theta\right] = \frac{1}{2\pi R}\int_{-\pi/2}^{+\pi/2}k_1^2\cos^2\theta|\hat{R}^{(1)}(k_1\sin\theta)|^2 d\theta + \frac{1}{2\pi R}\int_{-\pi/2}^{+\pi/2}k_2^2\cos^2\theta|\hat{R}^{(2)}(k_2\sin\theta)|^2 d\theta + O(1/R^2) \quad \text{(A3)}$$

Second, the wave functions $F_0^{(m)}(x,y)$ (2) in the polar coordinate system are given by:

$$F_0^{(1)}(R,\theta) = \exp\big(jk_1R\sin(\theta+\theta_i^{(1)}+\pi/2)\big) + \rho_{E_\parallel}^{(1)}\exp\big(jk_1R\sin(\theta-\theta_i^{(1)}-\pi/2)\big) \quad \text{(A4a)}$$

$$F_0^{(2)}(R,\theta) = \rho_{E_\parallel}^{(2)}\exp\big(jk_2R\sin(\theta+\theta_i^{(2)}+\pi/2)\big) \quad \text{(A4b)}$$

According to (A4) and taking into account the expression of Fresnel coefficients (3), we show the following result:

$$\mathrm{Im}\left[\int_{-\pi/2}^{+\pi/2}\left(F_0^{(1)}\frac{\partial F_0^{(1)}{}^*}{\partial r}+F_0^{(2)}\frac{\partial F_0^{(2)}{}^*}{\partial r}\right)d\theta\right] = 2\beta_i^{(1)}\big(|\rho_{E_\parallel}^{(1)}|^2-1\big)+2\beta_i^{(2)}|\rho_{E_\parallel}^{(2)}|^2=0 \quad \text{(A5)}$$

In a third stage, function $F_0^{(m)}(r,\theta)$ and its derivative $\frac{\partial F_0^{(m)}(r,\theta)}{\partial r}$ are expanded in a series of Bessel functions $J_n(k_mr)$, according to the following relation:

$$\exp(jk_mr\sin\delta) = \sum_{n=-\infty}^{+\infty}J_n(k_mr)\exp(jn\delta) \quad \text{(A6)}$$

with $\delta = \theta + \theta_i^{(1)} + \frac{\pi}{2}$, $\delta = \theta - \theta_i^{(1)} - \frac{\pi}{2}$ or $\delta = \theta + \theta_i^{(2)} + \frac{\pi}{2}$.

Using the asymptotic expansion of Bessel functions (A6) in relations (A4)

$$J_n(k_m r) = \sqrt{\frac{2}{\pi k_m r}} \left(\exp\left(jk_m r - j(2n+1)\frac{\pi}{4} \right) + \exp\left(-jkr_m + j(2n+1)\frac{\pi}{4} \right) \right) + O(r^{-3/2}) \tag{A7}$$

and taking into account far-field expression (6), the last two integrals are:

$$\mathrm{Im}\left[\int_{-\pi/2}^{+\pi/2} \left(F_0^{(1)} \frac{\partial F_d^{(1)\,*}}{\partial r} + F_d^{(1)} \frac{\partial F_0^{(1)\,*}}{\partial r} \right) d\theta \right] = \frac{2\beta_i^{(1)} \rho_{E_\parallel}^{(1)}}{R} \mathrm{Re}\big(\hat{R}_1(\alpha = k_1 \sin\theta_i^{(1)}) \big) + O(1/R^2) \tag{A8a}$$

$$\mathrm{Im}\left[\int_{-\pi/2}^{+\pi/2} \left(F_0^{(2)} \frac{\partial F_d^{(2)\,*}}{\partial r} + F_d^{(2)} \frac{\partial F_0^{(2)\,*}}{\partial r} \right) d\theta \right] = \frac{2\beta_i^{(2)} \rho_{E_\parallel}^{(2)}}{R} \mathrm{Re}\big(\hat{R}_2(\alpha = k_2 \sin\theta_i^{(2)}) \big) + O(1/R^2) \tag{A8b}$$

Integrals (A8) express the electromagnetic coupling between the scattered field $F_d^{(m)}(r,\theta)$ and the field without any deformation $F_0^{(m)}(r,\theta)$.

According to (A3), (A5) and (A8) and identifying the $\frac{1}{r}$ terms, the following relation can be derived from (A2):

$$\frac{1}{2\pi} \int_{-\pi/2}^{+\pi/2} k_1^2 |\hat{R}^{(1)}(k_1 \sin\theta) \cos\theta|^2 d\theta + \frac{1}{2\pi} \int_{-\pi/2}^{+\pi/2} k_2^2 |\hat{R}^{(2)}(k_2 \sin\theta) \cos\theta|^2 d\theta = -2\beta_i^{(1)} \rho_{E_\parallel}^{(1)} \mathrm{Re}\big(\hat{R}_1(\alpha = k_1 \sin\theta_i^{(1)}) \big) - 2\beta_i^{(2)} \rho_{E_\parallel}^{(2)} \mathrm{Re}\big(\hat{R}_2(\alpha = k_2 \sin\theta_i^{(2)}) \big) \tag{A9}$$

With the definition of the normalized angular power density (9), relation (A9) gives the power balance (10). The proof can also be applied to $H_\parallel$ polarized lossless media and gives the same power balance with the notation of fields (1) and (4).

REFERENCES

1. Chandezon, J., D. Maystre, and G. Raoult, "A new theoretical method for diffraction gratings and its numerical application," *J. Optics* (Paris), Vol. 11, 235–241, 1980.
2. Stratton, J. A., *Electromagnetic Theory*, McGraw-Hill, New York, 1941.
3. Elson, J. M. and R. H. Ritchie, "Photon interaction at a rough metal surface," *Phys. Rev.*, Vol. B4, 4129–4138, 1971.
4. Dusséaux, R. and R. de Oliveira, "Scattering of a plane wave by 1-dimensional rough surface — Study in a nonorthogonal coordinate system," *Progress in Electromagnetic Research*, Vol. PIER 34, 63–88, 2001.
5. Harrington, R. F., *Field Computation by Moment Methods*, McMillan, London, 1968.
6. Van Den Berg, P. M. and J. T. Fokkema, "The Rayleigh hypothesis in the theory of diffraction by a perturbation in a plane surface," *Radio Sci.*, Vol. 15, 723–732, 1980.
7. Millar, R. F., "The Rayleigh hypothesis and a related least-square solution to scattering problems for periodic surfaces and other scatterers," *Radio Sci.*, Vol. 8, 785–796, 1973.
8. Baudier, C. and R. Dusséaux, "Scattering of an $E_{\|}$-polarized plane wave by one-dimensional rough surfaces: Numerical applicability domain of a Rayleigh method in the far-field zone," *Progress in Electromagnetic Research*, Vol. PIER 34, 1–27, 2001.
9. Baudier, C. and R. Dusséaux, "Diffraction par une surface rugueuse diélectrique: Domaine d'application numérique d'une méthode de Rayleigh," *12th OHD Symposium*, 345–348, Le Mans, France, 2001.
10. Maystre, D., "Electromagnetic scattering from perfectly conducting rough surfaces in the resonance region," *IEEE Trans. Antennas Propagat.*, Vol. 31, No. 6, 885–895, 1983.
11. Maystre, D., "Rigorous theory of light scattering from rough surfaces," *J. Optics* (Paris), Vol. 15, No. 1, 43–51, 1984.
12. Maystre, D., O. Mata Mendez, and R. Roger, "A new electromagnetic theory for scattering shallow rough surfaces," *Optica Acta*, Vol. 30, No. 12, 1707–1723, 1983.
13. Tsang, L. and J. A. Kong, *Scattering of Electromagnetic Waves — Advanced Topics*, Ch. 1, Wiley Series in Remote Sensing, A Wiley-Interscience Publication, New York, 2001.